Banded sphalerite from the North Pennine Orefield

A. P. More

The Cavendish Laboratory, Madingley Road, Cambridge CB3 0HE

D. J. Vaughan

Department of Geology, The University of Manchester, Manchester M13 9PL

AND

J. R. Ashworth

School of Earth Sciences, The University of Birmingham, Edgbaston, Birmingham B15 2TT

Abstract

Optical microscopy of doubly polished thin sections of North Pennine sphalerite has revealed a range of previously unrecognised textures for the Alston Block mineralisation. Delicate growth zoning, interrupted by numerous solution disconformities, was seen in transmitted light. Two principal varieties of growth-banded sphalerite are recognised; the earlier (Type 1) is characterised by the development of thin opaque bands. Type 2 has colour bands between yellow and brown, correlated with iron content. In Type 1, iron levels (up to 3 wt.%) are not sufficient to account for the observed opacity. Ultra-violet and infra-red techniques failed to detect any organic inclusions. Electron microscopy revealed locally high concentrations of sub-micrometre inclusions, both beam-stable and beam-unstable, and a variety of growth-related crystal defects.

Fluid inclusion thermometry in both sphalerite varieties and the accompanying quartz gangue implies a saline mineralising fluid (20–25 wt.% equiv. NaCl) at a relatively low temperature (100° to 140 °C). Tubular inclusions are conspicuous. A deformation-induced lamelliform optical anisotropy is superimposed on a growth-related grid-iron anisotropy. Growth band offset is apparent where the deformation fabric cross-cuts the growth banding. Deformation on {111} twin and slip planes was indicated by electron microscopy.

Keywords: sphalerite, North Pennine orefield, zoning.

Introduction

Of the commonly occurring ore and gangue minerals, present in both hydrothermal veins and low-temperature Mississippi Valley Type (MVT) ores, sphalerite may be considered the most suitable for studies aimed at evaluating the conditions of mineralisation (Barton, 1982). Since it is translucent, doubly polished thin sections show additional textural information, especially the presence of internal banding, that is not apparent when using conventional polished blocks (Barton, 1978, Eldridge *et al.*, 1983). The banding may document fluctuations in the ore fluid chemistry or environment of deposition. Occasionally it may permit the recognition of a localised 'microstratigraphy' for the ore body (McLimans *et al.*, 1980). The compositional variations may be too slight to be detected by conventional analytical techniques (Craig and Vaughan, 1981). The study of solid and fluid inclusions may yield yet further information (Roedder, 1971, 1984).

Previous studies of the North Pennine Orefield, England have focused on gangue mineral assemblages (Dunham, 1948), ore mineral assemblages (Vaughan and Ixer, 1980) and possible ore origins (Brown *et al.*, 1987). Here, doubly polished thin sections are used to document a variety of growth-related textures, previously unreported, for the Alston Block part of the orefield.

Methodology

Principal experimental techniques are briefly detailed here. A fuller account is given in More

Mineralogical Magazine, September 1991, Vol. 55, pp. 409–416

(1988) and references therein. For microscopy in transmitted and reflected light, doubly polished thin sections were made, following Craig and Vaughan (1981). Thickness varied between 30 and 500 μm typically 100 to 150 μm. Thick samples enable delicate banding to be readily observed, and were made demountable for easy thermometric analysis of fluid inclusions, using a combined heating and freezing Linkam TH600 stage on a metallurgical microscope. Calibration against a range of organic standards to within 0.1 °C followed procedures of Shepherd *et al.* (1985).

Electron microprobe studies were carried out using a fully automated wavelength-dispersive, two-spectrometer, Cameca Camebax microprobe in the Dept of Geology, University of Manchester. Analytical conditions employed were a 20 kV, 14 nA beam, 60 second count times for majors, 100 second count times for traces, and a take-off angle of 40 degrees. Data were corrected using standard procedures (Reed, 1975), to a detection limit estimated at better than 0.02 weight percent.

Checks for an organic component were undertaken using ultra-violet optical microscopy and Fourier transform infra-red spectroscopy (FTIR). Conventionally polished blocks and doubly polished thin sections were examined in a Zeiss ultra-violet photo-microscope. FTIR spectroscopy in the spectral range 400 to 20 cm^{-1} used doubly polished thin sections. Samples of both banded and unbanded material were spectrally profiled using a computerised dedicated spectrometer at the Carnegie Institution, Geophysical Laboratory, Washington D.C.

Transmission electron microscopy (TEM) was carried out at 100 kV using a JEOL JM 100B. Samples were prepared from 30 μm thick doubly polished thin sections by ion-beam sputtering with a 5 to 6 kV argon beam, then coated with a 10 nm layer of carbon.

Samples

Material was obtained in situ from the lower levels of the Smallcleugh Vein and Handsome Mea Flats, and was supplemented by sampling of the tailings and dump material in the Nenthead District. The Nenthead mines and area are fully described in Dunham (1948). Material sampled comprised part of the assemblages detailed by Vaughan and Ixer (1980). The geology of the area is described fully in the literature, e.g. Dunham (1948), and well summarised by Ineson (1976).

Textural description

Mineralisation is developed in banded veins 1 to 10 cm wide. Set in a fractured silicified micrite, the coarsely crystalline veins chiefly comprise sphalerite and quartz. Optical microscopy shows two principal textural varieties of sphalerite; a widely developed type, here termed Type 2, and a patchily developed Type 1. Both are set in quartz gangue with minor siderite, galena, gersdorffite, pyrite and chalcopyrite.

Type 1 sphalerite is developed as a crustiform coating, varying in thickness from a few mm to 3 cm. Subhedral {111} and {1$\bar{1}$1} forms are observed in this paragenetically early phase, separated from the Type 2 mineralisation by a careous and irregular dissolution surface, which typically hosts lenses of gangue quartz with minor marcasite and gersdorffite. This sphalerite, unbanded in reflected light, is recognised in transmitted light by sub-parallel black (opaque) and grey bands typically less than 400 μm wide (Fig. 1). Between 3 and 8 prominent bands are recognised, which, when traced laterally for several cm through adjacent sphalerite crystals outline the crystal growth front during mineralisation. Locally some correlation of more brecciated and fragmented Type 1 sphalerite crystals is possible. Grey bands are optically translucent with no change in colour. Bands are observed bounded by two differing margins; one sharp and one diffuse. The sharp margin corresponds to the initial growth of the band, and is commonly decorated by irregular opaque inclusions up to 10 μm across. The diffuse margin, representing a return to more typical conditions, usually extends over several μm. Thicker bands tend to be composite with laterally discontinuous bands of a

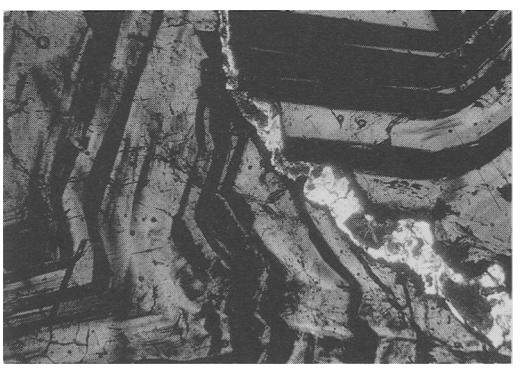

FIG. 1. Doubly polished thin section of Type 1 sphalerite. Well defined marker bands are seen tracing out the mineralisation growth. PPL Transmitted light. Field of view ~6600 μm.

few micrometres separation developed within the banded region (Fig. 2). Such regions are often dusted with numerous sub-micrometre inclusions and host thin rod-like inclusions parallel to crystal growth direction. Optically unidentifiable, such rods tend to nucleate from the initial sharply bounded margin. Where they intersect the polished surface no second phase is apparent but fine pitting is seen in reflected light (oil immersion), especially when the sample has been etched. The etchant used was 53% hydriodic with an etch time of three to four minutes, as detailed by Richards (1966).

Type 2 sphalerite is characterised by banding due to variations in body colour. This type accounts for more than 80 percent of the sphalerite sampled. Colour varied from a pale or honey yellow to deep red-brown with numerous intermediate shades. Colour banding traces out crystal growth. Band width ranges from a few hundred μm to more than 3 mm. Sharp colour changes typically correspond to either a dissolution surface or a later phase of mineralisation. Such discontinuities are frequent (Fig. 3). Early Type 2 bands tend to be dark, with later generations pale yellow. Sphalerite paragenesis is best illustrated by crystals isolated in the quartz gangue. A dark red–brown core, rarely hosting relict patches of Type 1, is separated from later pale yellow overgrowths by solution disconformities.

Both Types 1 and 2 sphalerite show complex, multiple sector zoning. Sector zoning is particularly well developed in the orange and pale yellow banded Type 2 material which additionally shows evidence for growth twinning. Where finely banded sphalerite is sector zoned and twinned, complex banded textures are developed (Fig. 4).

FIG. 2. Composite structure of banding within Type 1 sphalerite with sharp leading edges and diffuse trailing edges developed for the individual bands. Direction of crystal growth arrowed. PPL Transmitted light. Field of view ~890 μm.

Anisotropy and deformation. Both brittle and ductile deformational processes are inferred in both sphalerite and accompanying quartz mineralisation. Brittle deformation is apparent as brecciation and fracturing by both inter- and intra-grain cracks. Many microcracks within sphalerite end either at cleavage planes or as a series of narrow elongate fluid inclusions. Post-fracture healing of microcracks has commonly produced planes of secondary fluid inclusions.

Ductile deformation features are chiefly twin-planes, glide-planes, and subgrains. Throughout the sphalerite, a fabric comprising closely spaced sub-parallel twin and glide-planes is observed, both optically and by TEM. Optically this texture is apparent where it cuts delicately growth-banded areas, with band offset and changes in band width common. The twin and glide-planes principally develop along pre-existing growth twins and boundaries between sector zones. Reflected light microscopy of HI etched samples further shows this fabric developed in large areas of unbanded material. Subgrains, developed only in the more deformed and brecciated material, are best seen between crossed polars where optical anisotropy picks out the subgrain boundaries. In plane polarised light the subgrains are only apparent where a blotched or patchy colour is developed in otherwise delicately growth-zoned material.

Between crossed polars, most of the sphalerite is anisotropic. Three textural varieties are recognised: grid-iron, lamelliform, and undulose. Grid-iron anisotropy, developed throughout both deformed and undeformed sphalerite, is similar in optical appearance to the twinning of microcline feldspar (Fig. 6). Anisotropy is characterised as areas of numerous small diffuse laths set in two mutually perpendicular directions. Lath margins are sharp, but internally an undulose or diffuse extinction is seen.

Lamelliform anisotropy is associated with the deformation twin and glide-plane fabric. Laths are sharply bounded by sub-parallel planes tens of μm apart. Adjacent lamellae often show evidence for twinning, with uniform extinction. The effect is reminiscent of twinned plagioclase (Fig. 5). Undulose anisotropy is abundant throughout the sphalerite. It is characterised by areas of low birefringence showing undulose extinction. It occurs over hundreds of μm in the absence of deformation textures. In the more heavily deformed areas subgrain development is associated with an undulose anisotropy in patches less than 50 μm wide.

Electron microscopy. Textures observed by TEM reflect both growth and deformational

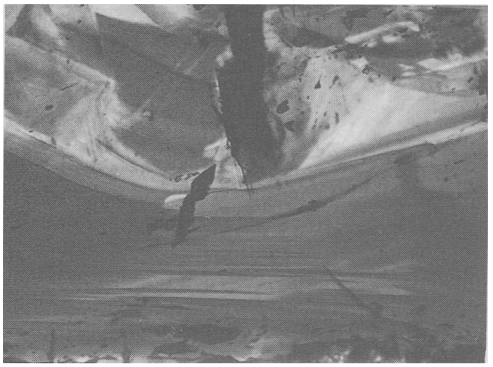

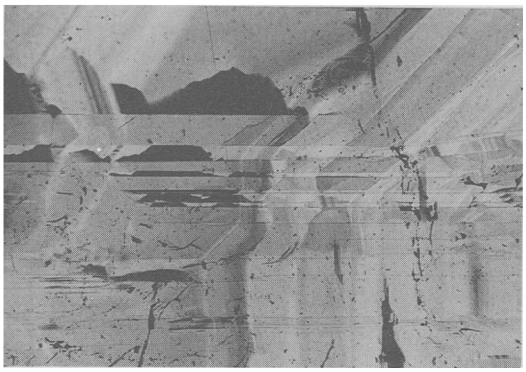

FIGS. 3 and 4. FIG. 3 (*left*). Type 2 banded sphalerite. The episodic nature of mineralisation is apparent with numerous discontinuities developed sub-parallel to banding. PPL Transmitted light. Field of view ~560 μm. FIG. 4 (*right*). Type 2 banded sphalerite showing textural modifications due to complex sector zoning and growth twinning. PPL Transmitted light. Field of view ~890 μm.

processes. Growth textures chiefly comprise crystal defects and microscopic inclusions. The defects are dislocation chains (a crystallographically-controlled line of 'point defects' having a chain-like appearance), stacking faults and point defects (or very tiny inclusions). Areas with a relatively high stacking-fault density also contain numerous 'point defects' with strain-fields in adjacent sphalerite. These defects are found in both sphalerite types, but Type 1 locally has the highest concentrations. Of the inclusions, some are stable in the electron beam and some unstable. Beam-stable ones are seen as anhedral patches of enhanced contrast, whereas beam-unstabled areas volatilise to leave a series of 1–3 μm rectangular voids with poorly developed corner facets. Associated with both kinds of inclusions are ribbon-like stacking faults and dislocation chains. Inclusions are sporadic in both Types 1 and 2 sphalerite.

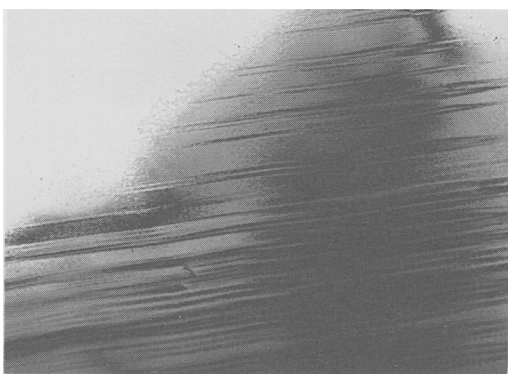

FIG. 5. Bright field electron micrograph of deformation-twinned type-two sphalerite. Field of view ~3.5 μm.

Unrelated to the above textures is a well developed, deformationally-induced microfabric. Both types of sphalerite host numerous {111} twin planes (Fig. 6). Unlike growth-related stacking faults, they form a strong unidirectional fabric parallel to the lamelliform optical anisotropy. Diffraction confirms a {111} composition plane for the twins. Twin-plane separation varies, typically in the range 0.25 to 1.0 μm. Maximum twin-plane density is locally estimated to exceed 15 000 planes per mm. Such twin-rich areas usually show a diffuse optical anisotropy.

Fluid inclusions

Both sphalerite types and the quartz gangue host a variety of primary and secondary inclusions, distinguished by the criteria of Roedder (1984), ranging in size from μm to several mm. Monophase primary (liquid or vapour), two-phase primary (liquid with vapour), and numerous secondary inclusions throughout the sphalerite are typically too small for reliable thermometric analysis, especially salinity determination. The larger primary inclusions show textural evidence for modification, with necking producing narrow and elongate inclusions. The majority of both primary and secondary sphalerite-hosted inclusions have been modified by fracture, twin and glide-plane development.

Tubular inclusions developed in the sphalerite, tens of μm to many hundreds of μm long, and up to tens of μm wide, occur in swarms along three mutually perpendicular directions (Fig. 7). The thinnest ones are indistinguishable from the rods mentioned above in the banded Type 1 sphalerite.

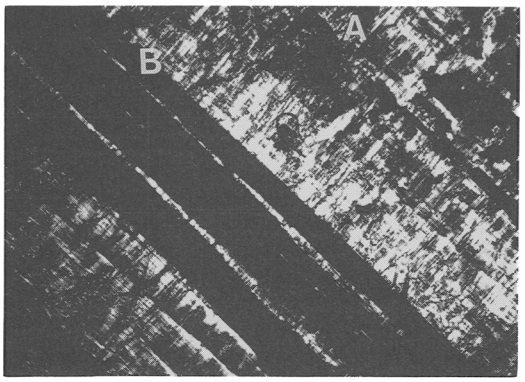

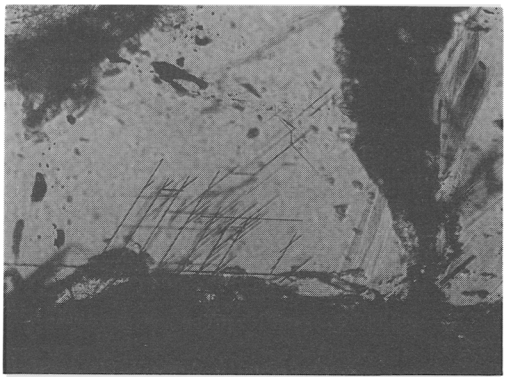

FIGS. 6 and 7. FIG. 6 (*left*). Region of Type 1 sphalerite with both grid-iron and lamelliform anisotropy developed. Areas of lamelliform anisotropy correlate with the planar fabric (A and B). XPL Transmitted light. Field of view ~2220 μm. FIG. 7 (*right*). Type 2 sphalerite containing numerous tubular inclusions. Three mutually-perpendicular tube directions are apparent, with arms developed for two of the three directions. PPL Transmitted light. Field of view ~225 μm.

Thermometric data. Homogenisation and freezing data from primary quartz-hosted inclusions, and with homogenisation data from suitable sphalerite-hosted primary inclusions, are presented in Table 1. No temperature differences were apparent for the two sphalerite types. For quartz-hosted inclusions, homogenisation data show a slight bimodal tendency, so two populations are inferred (Table 1) despite their optical similarity. The mean quartz-hosted freezing temperature ($T_{f\text{-mean}}$ −19.9 °C) corresponds to a fluid salinity of ~22.6 wt. percent equivalent NaCl (Potter and Brown, 1977). Homogenisation temperatures are reported uncorrected for possible overburden pressure effects.

Table 1

Thermometric data for primary fluid inclusions in quartz and sphalerite. T_h represents the temperature of homogenisation in degrees C, and T_f the temperature of last melting of ice (i.e. freezing) in degrees C. $T_{h\text{-}1}$ and $T_{h\text{-}2}$ refer to the two sphalerite-hosted inclusion populations recognised on the basis of measured homogenisation temperatures.

	Temperature Range (deg. C.)	Mean Temp (deg. C.)	No of Data Points	Standard Deviation
Quartz $T_{h\text{-}1}$	101.4 to 107.1	104.1	18	6.8
Quartz $T_{h\text{-}2}$	109.2 to 130.7	114.2	36	1.5
Quartz $T_{h\text{-}all}$	101.4 to 130.7	110.8	54	5.8
Quartz $T_{f\text{-}all}$	-22.3 to -17.1	-19.9	14	1.9
Sph. $T_{h\text{-}all}$	93.4 to 107.1	102.4	24	4.3

Compositional analysis

Ni, Co, and Ag were not detected. As was detected locally in Type 1 sphalerite; As and Sb were detected at very low levels in Type 1 sphalerite. The minor elements Fe and Cd are higher in banded than in unbanded Type 1 (Fig. 8). They are possibly correlated (Fig. 9*a*), as are the trace elements copper and antimony (Fig. 9*b*) though these show no association with the banded regions.

In Type 2 sphalerite iron and cadmium were detected in minor amounts. Levels of iron corre-

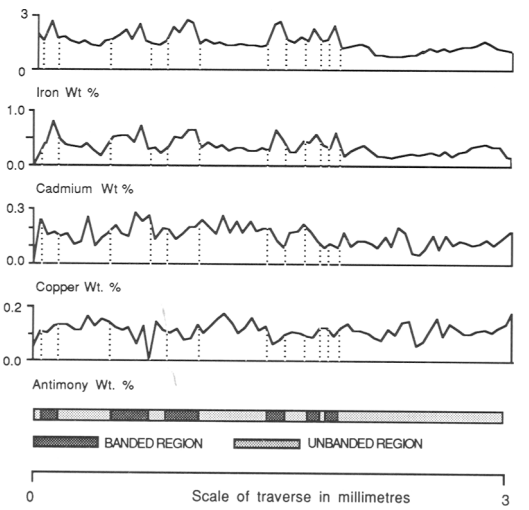

FIG. 8. Elemental compositional traverses across a banded region of Type 1 sphalerite.

late with sphalerite body colour. Low levels (1 to 2 wt.%) occur in the pale yellow sphalerite, whilst the highest levels (5+ wt.%) are recorded from the dark orange and red–brown sphalerite. Cadmium correlates with iron (Fig. 9*c*). The trace quantities of copper, however, show an inverse correlation, with the highest levels (0.35 wt.%) in the pale yellow sphalerite.

A traverse across a dissolution surface between Types 1 and 2 shows Type 2 to be enriched in iron (Fig. 10). The converse is true for cadmium. Type 1 is relatively rich in antimony and copper, with the highest concentrations recorded at the dissolution surface dividing the two types.

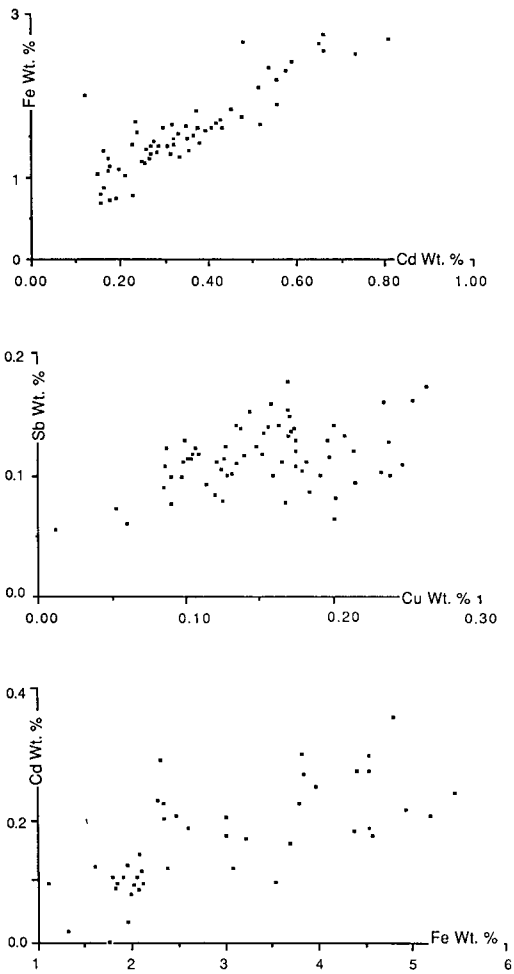

FIG. 9. Elemental variation diagrams for Types 1 and 2 sphalerite: (*a*) Type 1: Cadmium versus Iron (*b*) Type 1: Copper versus Antimony (*c*) Type 2: Cadmium versus Iron.

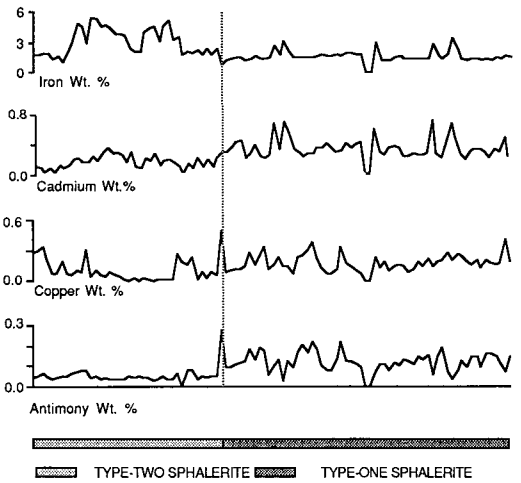

FIG. 10. Element compositional traverses for adjacent regions of Type 1 and 2 sphalerite separated by a dissolution surface.

Discussion

Mineralisation was episodic. Fluid composition alternated between supersaturated with respect to sphalerite (deposition) and undersaturated (dissolution). Subtle changes in fluid composition are indicated by the zoning. Textural evidence for extreme levels of fluid supersaturation (e.g. colloform, fibrous, or very tiny crystals) or undersaturation (e.g. relict grains) are absent. Barton *et al.* (1963) suggested that texturally similar sphalerite in the Creede epithermal-vein orefield was deposited under quasi-equilibrium conditions, with ZnS concentration in solution varying just above and below saturation level.

The fluid inclusion work indicates a low-temperature, highly saline, mineralising fluid. Salinities greater than 20 equiv. weight percent NaCl are indicated. The range of freezing temperatures encompasses the eutectic temperature (−20.8 °C) for the NaCl–water system implying the presence of other salts in solution in addition to NaCl (Roedder, 1984). A possible Ca or Mg component is not unexpected in view of the widespread fluorite and carbonate mineralisation throughout the North Pennine Orefield. Homogenisation temperatures should be corrected for overburden pressure to give true mineralisation temperatures. Based on a maximum estimated overburden of 1100 metres, Sawkins (1966) suggests a mean overburden pressure of 200 bars, giving a temperature correction of +11 °C with uncertainty ±11 °C. Using the data of Haas (1976) and Potter and Brown (1977), and 1100 metres over-burden pressure, a corrected

temperature for mineralisation of 122 ± 12 °C may be suggested (More, 1988). This is significantly lower than the 250 °C reported for the Alston Block cupola mineralisation (Vaughan and Ixer, 1980). The Nenthead samples examined reflect this low mineralisation temperature in the low iron content of the sphalerite and the relatively simple mineralogy of the deposit. The presence of pyrite and absence of pyrrhotine supports a low temperature of mineralisation in line with the phase relations show in Fig. 11. It should be emphasised that the phase relations presented here are tentative, and not demonstably equilibrium phase boundaries; nevertheless they are illustrative of the overall *T–X* relations in this system.

Texturally Type 2 sphalerite is not atypical of MVT ores and low temperature hydrothermal veins. The opaque-banded Type 1 is unusual, and has not previously been described from the North Pennine Orefield. In similar material from the Pine Point Deposit (Roedder and Dwornik, 1968), compositional banding is discounted, and various possible band origins involving crystal growth defects and inclusion contents discussed. The Nenthead Type 1 material is enriched in a range of trace metals not normally reported for MVT sphalerites (Hagni, 1983): antimony, copper, and arsenic. A compositional origin for the banding is ruled out, as follows. Observed changes in iron concentration, developed across the well developed banded regions, i.e. approximately 1 to 2 mole percent, are insufficient to cause opacity, which requires more than 8 mole percent according to McLimans *et al.* (1980). Copper, antimony and arsenic show no correlation with the banded Type 1 regions. Cadmium, the only other metal detected in significant quantities, should have little effect on sphalerite body colour (Boldish, 1973).

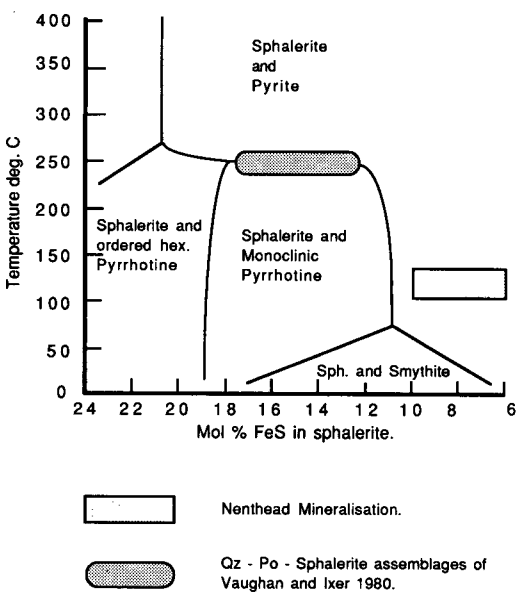

FIG. 11. Schematic phase diagram showing a *T–X* projection of part of the FeS–ZnS system. Modified from Scott and Kissin (1973) and Vaughan and Ixer (1980).

Type 1 sphalerite is similar to hydrocarbon-bearing banded material in several MVT deposits (e.g. Foley, 1980). Hydrocarbon-banded sphalerite typically shows cadmium enrichment in the banded regions (Craig *et al.*, 1983), as in Nenthead Type 1 material. However both UV microscopy and FTIR spectroscopy of both banded and unbanded Type 1 regions have failed to detect any carbon or hydrocarbon component. FTIR absorption spectra in the regions 3000 to 2700 cm^{-1} (methyl and ethyl groups), 2700 cm^{-1} (aromatic groups), and 1750 to 1700 cm^{-1} (C=O groups) of banded and unbanded regions are identical and free of absorption bands characteristic of the above functional groups.

Optically, there are similarities between the less well developed Type 1 bands and the 'bead chain' textures of Barton and Bethke (1987) which are rod-like inclusions in large, delicately growth-zoned sphalerite crystals, and are interpreted as primary growth features. Rod and inclusion morphology in the Nenthead examples is simpler. The rods may change direction, but do not form complex tetrahedral patterns like those described by Barton and Bethke (1987). One possible origin for the Nenthead rod-like inclusions is that of growth defects (chain-like dislocations) being 'carried' by the crystal face during growth. Such a defect would then be drawn out in the direction of crystal growth. Crystallographically-controlled dislocation slip oblique to the growth direction could generate the rod-like defects inclined to growth banding. 'Blotching' of the rods, attributed to defect decoration by Barton and Bethke (1987), possibly by Cu–Fe sulphides, is absent for all but a few of the rods seen. Blotched rods are best observed in remnant patches of a deep red-brown, iron-rich, Type 1 material which, however, lacks Cu-Fe sulphide phases. The slight increase in trace metal concentrations in a banded region may reflect localised decoration of point and chain-like defects by other mineral phases. Crystal defects are preferred sites for the nucleation of a second phase because they reduce the activation energy required for the second phase to nucleate. TEM shows Type 1 sphalerite to be rich in both "point" and planar defects, along with numerous un-

identified inclusions. A locally high concentration of such defects and inclusions could potentially render the sphalerite opaque.

Two end-member anisotropic textures are recognised: growth induced 'grid-iron' and deformational 'lamelliform' anisotropy. The origin of the third or undulose variety is less clear. Studies of undeformed Appalachian ores (More, 1988; Seal *et al.*, 1985) show undulose anisotropy of a growth origin, attributed to primary stacking disorder and other growth defects developed within the sphalerite. Defect-rich sphalerite, Type 1 of this study for instance, could be expected to exhibit an undulose anisotropy in addition to grid-iron anisotropy but interpretation is made difficult by the deformation. Lattice strain, along with deformation twinning, may induce undulose anisotropy. Possibly such regions are areas which have undergone recovery by sub-grain development.

Conclusion

The use of doubly polished thin sections permits examination of a variety of growth related textures in the Nenthead sphalerite. Two banded varieties are distinguished. Type 2 has colour banding due to fluctuations in the composition. The paragenetically early Type 1 is growth-banded with opaque horizons, which are probably due to localised concentration of inclusions and crystal defects. Textural, compositional and fluid inclusion evidence for both sphalerite types implies a low-temperature highly saline brine for the mineralising fluid, with only moderate saturation levels of ZnS.

The refractory nature of sphalerite enables preservation of the growth-related textures despite post-mineralisation deformation. A range of deformation-induced microstructures including a distinctive optical anisotropy modify the growth-related textures but are easily distinguished from them.

Acknowledgements

One of us (APM) would like to acknowledge the support of the NERC through a research studentship. The staff of the Department of Geology, University of Aston, are thanked, as are Dave Plant and Tim Hopkins from the Department of Geology, University of Manchester, for their assistance with the microprobe analyses. Also thanked are Dr. A. Gize, University of Manchester, for the FTIR spectrometry, and Dr D. Manning, University of Manchester, for assistance with the UV microscopy.

References

Barton, P. B. (1978) *Mining Geol.*, **28**, 293–300.

——(1982) *Min. Soc. Bull.* (London), no. 57, 3–4.

——and Bethke, P. M. (1987) *Am. Mineral.*, **72**, 451–67.

——Bethke, P. M., and Toulmin, P. (1963) *Min. Soc. America. Special Paper*, **1**, 171–85.

Boldish, S. I. (1973) *Relation of the Band Gap to Crystal Chemical Parameters.* Unpublished M.Sc. thesis, Pennsylvania State University.

Brown, G. C., Ixer, R. A., Plant, J. A., and Webb, P. C. (1987) *Trans. Inst. Mining Metall. (Sect. B: Appl. Earth Sci.)*, **96**, B65–B76.

Craig, J. R. and Vaughan, D. J. (1981) *Ore microscopy and Ore Petrography*. Wiley, New York. 406pp.

——Solberg, T. N., and Vaughan, D. J. (1983) *Int'l Conference on Mississippi Valley-type Lead Zinc Deposits*, proceedings volume. (Kisvarsanyi, G. *et al.*, eds.) University of Missouri-Rolla, 317–27.

Dunham, K. C. (1948) *Geology of the Northern Pennine Orefield.* Vol. 1, *Tyne to Stainmore.* Mem. Geol. Survey U.K., H.M.S.O., London. 375pp.

Eldridge, C. S., Barton, P. B., and Ohmoto, H. (1983) *Economic Geology Monograph 5*: The Kuroko and related volcanogenic massive sulfide deposits, 241–81.

Foley, N. K. (1980) *Mineralogy and Geochemistry of the Austinville–Ivanhoe District. Wythe County, Virginia.* M.Sc. thesis, Virginia Polytechnic Institute and State University, Blacksburg, 83pp.

Hagni, R. D. (1983) In *Unconventional Mineral Deposits* (Shanks, W., ed.) Soc. Mining Engineers, AIMME, 71–88.

Hass, J. L. (1976) *U.S. Geol. Surv. Bull.* 1421-A, U.S. Dept. Interior, Washington.

Ineson, P. R. (1976.) In *Handbook of Stratabound and Stratiform Ore Deposits* (Wolf, K. L., ed.) Elsevier, Amsterdam, **5**, 197–230.

McLimans, R. K., Barnes, H. L., and Ohmoto, H. (1980) *Econ. Geol.*, **75**, 351–62.

More, A. P. (1988) *Textural and Microstructural Studies of Zinc Sulfide and Associated Phases in Certain Base Metal Deposits.* PhD. thesis. Univ. of Aston in B'ham. 257pp.

Potter, R. W. and Brown, D. L. (1977) *U.S. Geol. Surv. Bull.* 1421-C, U.S. Dept. Interior, Washington.

Reed, S. J. B. (1975) *Electron Probe Microanalysis.* Cambridge University Press, Cambridge.

Richards, S. M. (1966) *C.S.I.R.O., Techn. Publ.*, **5**. 27pp.

Roedder, E. (1971) *Econ. Geol.*, **66**, 777–91.

——(1984) *Reviews in Mineralogy*, Volume 12. Series Editor, Ribbe, P. H. Min. Soc. America, Blacksburg, Virginia. 644pp.

——and Dwornik, E. J. (1968) *Am. Mineral.*, **53**, 1523–9.

Sawkins, F. S. (1966) *Econ. Geol.*, **61**, 385–401.

Scott, S. D. and Kissin, S. A. (1973) Ibid. **68**, 475–9.

Seal, R. R., Cooper, B. J., and Craig, J. R. (1985) *Can. Mineral.*, **23**, 83–8.

Shepherd, T., Rankin, A. H., and Alderton, D. H. M. (1985) *Fluid Inclusion Studies.* Blackie, London. 239pp.

Vaughan, D. J. and Ixer, R. A. (1980) *Trans. Inst. Mining Metall. (Sect. B: Applied Earth Sciences)*, **89**, B99–B110.

[*Revised manuscript received 25 March 1991*]